Derivation of enhanced potentials for cerium brannerite and the calculation of lattice and intrinsic defect properties

Read, Mark; Bird, Rebecca

DOI:
10.1016/j.nimb.2016.10.015

Document Version
Peer reviewed version

Citation for published version (Harvard):
Read, M & Bird, R 2016, 'Derivation of enhanced potentials for cerium brannerite and the calculation of lattice and intrinsic defect properties', *Nuclear Instruments & Methods in Physics Research. Section B. Beam Interactions With Materials and Atoms*. https://doi.org/10.1016/j.nimb.2016.10.015

Nuclear Instruments and Methods in Physics Research B xxx (2016) xxx–xxx

Contents lists available at ScienceDirect

Nuclear Instruments and Methods in Physics Research B

journal homepage: www.elsevier.com/locate/nimb

Derivation of enhanced potentials for cerium brannerite and the calculation of lattice and intrinsic defect properties

Rebecca A. Bird, Mark S.D. Read *

School of Chemistry, University of Birmingham, Edgbaston, Birmingham B15 2TT, United Kingdom

ARTICLE INFO

Article history:
Received 2 August 2016
Received in revised form 6 October 2016
Accepted 10 October 2016
Available online xxxx

Keywords:
Ceriumn brannerite
Atomistic simulation
Potentials
Novel methodology

ABSTRACT

A new potential has been derived for ceria and used to calculate its lattice and defect properties. The $Ce^{4+} \cdots O^{2-}$ potential is obtained *via* a combination of empirical fitting to crystal structural data and parametric fitting to additional physical properties, while the $O^{2-} \cdots O^{2-}$ potential is transferred from earlier publications on UO_2 and PuO_2. The overall potential is subsequently verified and validated by calculation of elastic and dielectric constants, whose values agree favourably with those measured experimentally. The potential is then employed to calculate intrinsic defect formation energies and predict the most favourable type of intrinsic disorder.

1. Introduction

High Level Waste (HLW), containing up to 95% of the radioactivity associated with a nuclear power station [1], comprises energetic fission products many of which have long half-lives and must therefore be isolated from the biosphere [2]. Borosilicate glass is currently the most commonly employed immobilizing matrix. However, the limited solubility of some HLW components and suggestions of inhomogeneity of the borosilicate matrix, has led to active research of ceramics, particularly those with mineral analogues, as alternative host matrices [3].

The mineral brannerite, UTi_2O_6, has a high actinide content and is extremely durable despite a wide variety of chemical substitution on both cation sites [4]. Synthetically, brannerite is a significant minor phase in pyrochlore-zirconolite ceramics designed for HLW immobilization [5]. It is therefore important to consider the applicability of brannerite as an actinide immobilizing matrix. Cerium is often used as an actinide simulant [6], particularly for plutonium, and $CeTi_2O_6$ is iso-structural with both UTi_2O_6 and $PuTi_2O_6$ [7].

Included in the detailed study of the structural properties of $CeTi_2O_6$ by Stennett et al. [7], are atomistic simulations employing potentials from the library of Woodley et al.[8] However, the reported results were not reproducible with the listed potentials. Moreover, the interatomic potential employed for the anion interactions includes an attractive r^{-6} term that causes unphysical and catastrophic attraction when the anions are separated by less than 1.85 Å. In addition, as seen when other potentials from the same library were used in the simulation of κ-alumina [9], these potentials give rise to further anomalies.

In this study, methods similar to those adopted previously for UO_2 [10] are applied to CeO_2 in order to obtain information about lattice properties and defect behaviour. This is an important preliminary step in modelling cerium brannerite which is the subject of ongoing work and a future publication.

2. Computational methodology

The computational methods used in this work are established techniques that have been used in many applications [11,12]. The pairwise interactions in the material are defined by a linear sum of an electrostatic interaction term and an interatomic potential (Eq. (1)):

$$V_{ij} = \underbrace{A_{ij}\ \exp\left(-\frac{r_{ij}}{\rho_{ij}}\right) - \frac{C_{ij}}{r_{ij}^6}}_{\text{Buckingham}} \underbrace{+\frac{q_i q_j}{r_{ij}}}_{\text{Electrostatic}} \quad (1)$$

For the interatomic potential term, the Buckingham form is employed in which q_i and q_j are the formal charges on the ions and the parameters A, ρ and C are specified, through empirical fitting, for each interaction type. Ion polarization by highly charged

* Corresponding author.
E-mail address: m.s.d.read@bham.ac.uk (M.S.D. Read).

http://dx.doi.org/10.1016/j.nimb.2016.10.015
0168-583X/

ions and defects is incorporated using Dick and Overhausers shell model [13] and intrinsic defects are modelled with the computationally efficient Mott Littleton [14] procedure.

2.1. Anion – anion potential

The interactions between the anions are described using a Buckingham four range potential: this was reported for UO_2 [10,15] and has subsequently been used in simulations of SiO_2 [16], PuO_2 [17] and ThO_2 [18]. Its use here is reasonable as CeO_2 adopts the same cubic crystal structure, with the anions arranged with the same symmetry within unit cells of a similar size. The potential is defined by the intervals given in Eq. (2) such that only the relevant terms of the Buckingham function are used over specific interaction distances. At the points $\text{cut}_1, r_{\text{minimum}}$ and cut_2, the functions are splined such that their first and second derivatives are continuous. Furthermore, the function is constrained to have a minimum stationary point at r_{min}. Values for the necessary parameters, are reported by Jackson et al. and the constants for the polynomials calculated using the spline fitting procedure embodied within the GULP [19] code.

$$\phi^{\text{Buck4}}(r_{ij}) = \begin{cases} A_{ij}\exp\left(-\frac{r_{ij}}{\rho_{ij}}\right) & \text{if } r_{\text{min}} < r_{ij} \leqslant \text{cut}_1, \\ \sum_{m=0}^{5} a_m\, r_{ij}^m & \text{if } \text{cut}_1 < r_{ij} \leqslant r_{\text{minimum}}, \\ \sum_{n=0}^{3} b_n\, r_{ij}^n & \text{if } r_{\text{minimum}} < r_{ij} \leqslant \text{cut}_2, \\ -\frac{C_{ij}}{r_{ij}^6} & \text{if } \text{cut}_2 < r_{ij} \leqslant r_{\text{max}} \end{cases} \tag{2}$$

2.2. Cation – anion potential

Owing to the absence of a stationary point in the function of the cation–anion interactions, the Buckingham four range potential form is thus not applicable. To the best of the authors knowledge, there exists no standard Buckingham form potentials for $Ce^{4+} \cdots O^{2-}$ interactions that are consistent with the Buckingham four range potential detailed above. Thus, this is derived, with the C parameter set to zero in order to overcome the unphysical phenomenon of catastrophic attractions when ions are in close proximity: the potentials are thus formally of the Born Mayer form. The nature of the excluded $(-C/r^6)$ term is incorporated by surveying the potential landscape and sequentially selecting A and ρ parameters using an empirical fitting procedure which requires no *a priori* assumption of starting values and has been used to derive potentials for use in simulations of UO_2 [10], PuO_2 [17] and ThO_2 [18].

Initially, a range of A (650–2000 eV) and ρ (0.30–0.45Å) values is screened and the difference between the experimentally observed and predicted lattice constant plotted in Fig. 1.

Interpolation of the surface for where this difference is zero provides a solution set (Fig. 2) of several pairs of A and ρ that accurately reproduce the crystal structure.

For a robust model, however, the physical characteristics of the lattice should be described. Therefore, the predicted elastic constants are plotted as a function of the A parameter of corresponding pairs in the solution set (Fig. 3 and a value of A selected where the mean percentage difference between the predicted and observed values (overlaid in Fig. 3) of the elastic constants is a minimum. The corresponding ρ value is obtained through interpolation of the solution set.

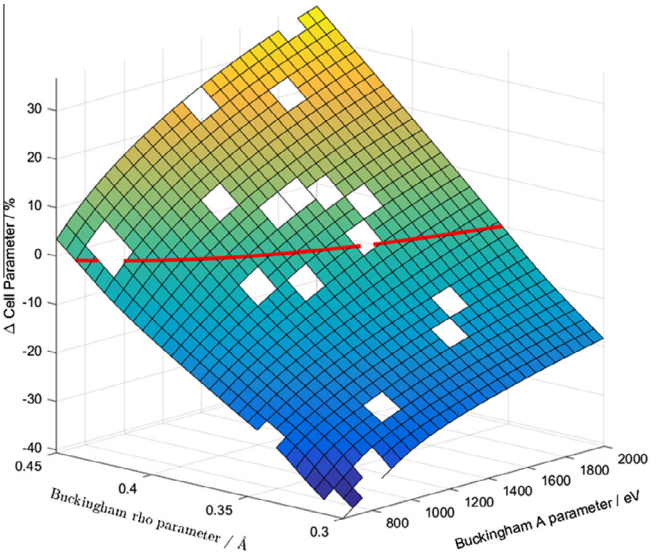

Fig. 1. Plot of the difference between predicted and observed CeO_2 lattice constant for A and ρ values of the $Ce^{4+} \cdots O^{2-}$ Born–Mayer potential.

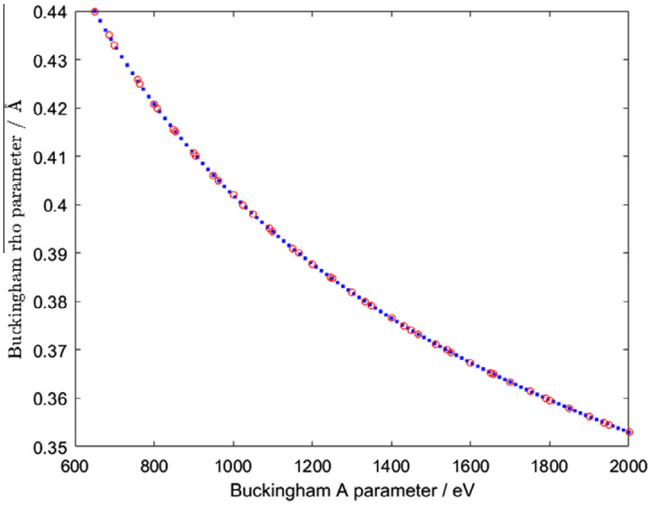

Fig. 2. Zero contour points and interpolated values of A and ρ comprising the solution set.

3. Results and discussion

3.1. Experimental data

CeO_2 adopts the fluorite structure ($Fm\bar{3}m$) and is isomorphous with UO_2, PuO_2 and ThO_2. The face centred cubic lattice has a lattice constant, a_0, of 5.4112Å [20] and a basis of a cerium ion at the origin and oxygen ions at $\pm(\frac{1}{4},\frac{1}{4},\frac{1}{4})$: the anions form a simple cubic sub-lattice. There are 4 cations and 8 anions per unit cell. The fitting procedure also employs the elastic constants (C_{11}, C_{12} and C_{44}), static and high frequency dielectric constants and these are summarised, along with other bulk properties to be used for validating the simulation, in Table 2.

3.2. Perfect lattice

Values for the parameters of the $Ce^{4+} \cdots O^{2-}$ potential derived in the previous section and the Buckingham four range $O^{2-} \cdots O^{2-}$ potential are given in Table 1.

Please cite this article in press as: R.A. Bird, M.S.D. Read, Derivation of enhanced potentials for cerium brannerite and the calculation of lattice and intrinsic defect properties, Nucl. Instr. Meth. B (2016), http://dx.doi.org/10.1016/j.nimb.2016.10.015

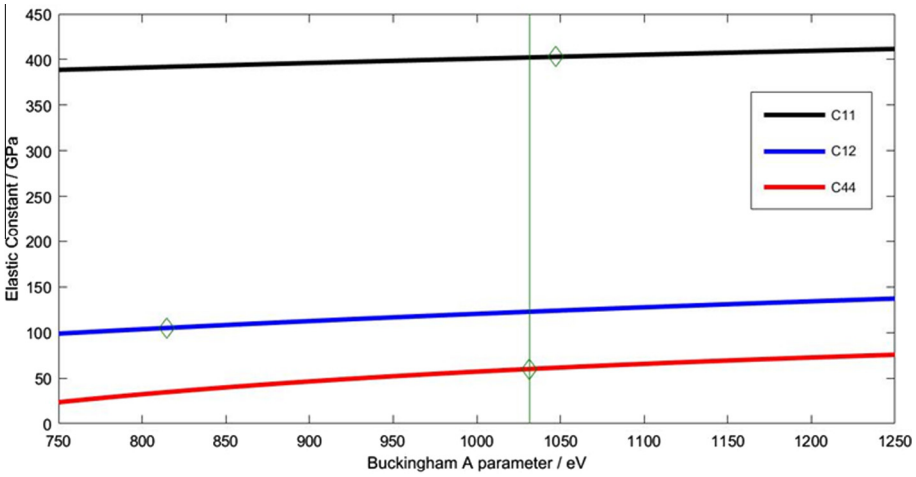

Fig. 3. Plot of predicted and observed elastic constants as a function of *A*.

Table 1
Lattice potentials for CeO_2.

Interaction	Short-range parameters			Shell model*	
	A eV	ρ Å	C eV Å^6	Y $\|e\|$	k_2 eV Å^{-2}
$Ce^{4+}\ldots O^{2-}$	1031.57	0.399447	0.0	−2.54	105.358
$O^{2-}\ldots O^{2-}$ [(a)]	11272.6	0.1363	134.0	−4.4	296.2
	r_{min} Å 0.0	cut_1 Å 1.2	$r_{minimum}$ Å 2.1	cut_2 Å 2.6	r_{max} Å 15.0

* Y and k_2 are the shell charge and spring constant respectively
(a) Reference [15]

The validity of the potentials used and the applicability of the model is assessed by comparing the predicted values of perfect lattice properties with those that have been experimentally observed. Table 2 shows excellent agreement between calculated parameters and reported crystallographic data, elastic constants and both static and high frequency dielectric constants. However, such good agreement is not surprising as these properties were used in the potential derivation: further validation of the model is thus carried out through consideration of additional properties listed in Table 2, with prediction once again being compared with reported observation. Comparison with potentials [8,21–26] taken from the literature shows the parameterisation used in this work to be an improved fit.

3.3. Intrinsic defects

Calculations were performed initially on the energies of isolated point defects: results are given in Table 3. In all cases, the lattice ions surrounding the defect are allowed to relax in the energy minimisation procedure using the Mott-Littleton procedure [14], in which the immediate surroundings of the defect are treated explicitly and approximations used for more distant regions: consistent region sizes of 14 Å and 28 Å were used, giving ≈1800 ions in region 1 and ≈12,300 ions in region 2.

Frenkel and Schottky disorder formation energies are predicted by combining individual point defect energies. However, this assumes the defects are at infinite dilution and does not take into account the binding energy associated with defect aggregation. This is addressed by performing cluster calculations: the binding energies are then determined as the difference in energy between the cluster and its constituent point defects at infinite dilution.

3.3.1. Frenkel pair clusters

Using Kröger Vink notation [35] notation, Frenkel defects can be represented as:

$$\begin{aligned} Ce_{Ce}^{\times} &\rightleftharpoons V_{Ce}'''' + Ce_i^{\bullet\bullet\bullet\bullet} \\ O_O^{\times} &\rightleftharpoons V_O^{\bullet\bullet} + O_i'' \end{aligned} \tag{3}$$

For the oxygen Frenkel cluster simulations, the interstitial and vacancy are separated by a cerium ion in order to prevent the recombination seen when the defects are in close proximity. Two geometries for the oxygen Frenkel Pair are considered and the respective coordinates and resulting energies listed in Table 4.

3.3.2. Schottky defect clusters

Using Kröger Vink notation, Schottky defects are represented as:

$$Ce_{Ce}^{\times} + 2O_O^{\times} \rightleftharpoons V_{Ce}'''' + 2V_O^{\bullet\bullet} + CeO_2(\text{Surf.}) \tag{4}$$

In a similar manner to that used for the oxygen Frenkel pairs, three configurations of the trio of vacancies in Schottky disorder were simulated. In all three configurations, the cerium vacancy is positioned at $(0,0,0)$ and the first oxygen vacancy positioned at $(0,0,0)$. The coordinates of the second oxygen vacancy, which preserves charge neutrality, and the associated energies are given in Table 5. The most energetically favourable position for the second oxygen vacancy is predicted to be that of the Sch. 2 configuration and this cluster energy is combined with the associated energy of forming CeO_2 at the surface to predict the Schottky defect energy detailed in Table 6.

Formation energies for Frenkel and Schottky disorder, found from both combining point defect energies and cluster calculations, are given in Table 6. It can be seen that for all defect types

Please cite this article in press as: R.A. Bird, M.S.D. Read, Derivation of enhanced potentials for cerium brannerite and the calculation of lattice and intrinsic defect properties, Nucl. Instr. Meth. B (2016), http://dx.doi.org/10.1016/j.nimb.2016.10.015

Table 2
Comparison of predicted and observed properties of CeO_2.

Property	Observed	This work	Δ %	Butler [21]	Δ %	Gotte [22]	Δ %	Woodley [8]	Δ %	Minervini [23]	Δ %	Vyas [24]	Δ %	Li [25]	Δ %	*Ghosh** [26]	Δ
Lattice Constant:																	
(a_0) (Å)	5.4112	5.4114	0.004	5.4677	1.044	5.4070	−0.078	5.4110	−0.004	5.4100	−0.022	5.4110	−0.004	5.4080	−0.059	5.3960	−0.281
Elastic Constants:																	
C_{11} (GPa)	403[(b)]	402.3	−0.17	490.2	21.64	405.5	0.62	587.8	45.86	554.5	37.59	573	42.18	503.7	24.99	410.5	1.86
C_{12} (GPa)	105[(b)]	122.8	16.95	140.6	33.90	104.3	−0.67	111.3	6.00	124.6	18.67	147.7	40.67	143.9	37.05	79.2	−24.57
C_{44} (GPa)	60.0[(b)]	60	0.00	132.4	120.67	60.6	1.00	61.6	2.67	123.1	105.17	146.8	144.67	143.7	139.50	78.5	30.83
Moduli:																	
Bulk (GPa)	204 – 240[(c)]	215.96		257.13		204.71		270.15		267.92		289.42		263.83		189.61	
Shear (GPa)	96 – 149[(d)]	91.9		149.37		96.58		132.26		159.85		173.12		158.17		113.35	
Young's (GPa)	249[(b)]	344.86		427.52		362.79		552.34		508.78		512.45		439.68		384.94	
Dielectric Constants:																	
Static ε_0	23 – 35.3[(e)]	26.73		22.52		18.721		11.26		18.62		12.71		10.41		4.615	
High Frequency ε_∞	4.7 – 6.0[(e)]	5.518		5.415		4.012		4.23		5.88		3.98		1.09			

(a) Reference [20], (b) Reference [27], (c) Reference [28–31], (d) Reference [27,28], (e) Reference [32,33,34], ∗ Partial charge model.

Table 3
Defect formation energies for isolated defects in CeO_2

Defect	Position	Formation Energy/ eV
Ce^{4+} Vacancy (V''''_{Ce})	(0,0,0)	78.60
O^{2-} Vacancy ($V^{\bullet\bullet}_{O}$)	$(\frac{1}{4},\frac{1}{4},\frac{1}{4})$	16.37
Ce^{4+} Interstitial ($Ce^{\bullet\bullet\bullet\bullet}_{i}$)	$(\frac{1}{2},\frac{1}{2},\frac{1}{2})$	−61.66
O^{2-} Interstitial (O''_{i})	$(\frac{1}{2},\frac{1}{2},\frac{1}{2})$	−11.87

Region I contains 1800 ions.

Table 4
Formation and binding energies of the considered configurations for the oxygen Frenkel pair defect.

Type of defect	$V^{\bullet\bullet}_{O}$ Position	O''_{i} Position	Formation energy (eV/Defect)	Binding energy (eV/Defect)
OFP 1	$(-\frac{1}{4},-\frac{1}{4},-\frac{1}{4})$	$(\frac{1}{2},\frac{1}{2},\frac{1}{2})$	1.55	−0.70
OFP 2	$(-\frac{1}{4},-\frac{1}{4},\frac{1}{4})$	$(\frac{1}{2},\frac{1}{2},\frac{1}{2})$	1.86	−0.40

Table 5
Formation and binding energies of the Ce^{4+} and 2 O^{2-} vacancy clusters.

Type of defect	Second $V^{\bullet\bullet}_{O}$ Position (eV/Defect)	Formation energy	Binding Energy (eV/Defect)
Sch. 1	$(-\frac{1}{4},-\frac{1}{4},-\frac{1}{4})$	35.95	−1.17
Sch. 2	$(-\frac{1}{4},\frac{1}{4},-\frac{1}{4})$	35.92	−1.19
Sch. 3	$(-\frac{1}{4},\frac{1}{4},\frac{1}{4})$	36.12	−0.99

Table 6
Calculated formation and binding energies of the ionic defects in CeO_2.

Type of defect	Defect formation energy		Binding Energy (eV/Defect)
	Unbound (eV/Defect)	Bound (eV/Defect)	
Ce Frenkel	8.47	6.71	−1.77
O Frenkel	2.25	1.86	−0.40
Schottky Trio	2.78	1.59	−1.19

there is a net binding energy. It is also interesting to note that consideration of only defects at infinite dilution would lead to the conclusion that oxygen Frenkel disorder, having the lowest formation energy and thus being the most thermodynamically stable, would dominate. When defect aggregation is taken into account, however, the Schottky trio of vacancies is predicted to have the lowest formation energy. Thus, cerium and oxygen vacancies are expected in the structure in accord with observation.

4. Conclusions and future work

A potential has been fitted to the structure and properties of CeO_2 using a robust procedure to ensure the crystallographic and mechanical properties are reproduced accurately. Starting from a solution set of parameters which correctly reproduce the crystallographic structure, values are selected based on their ability to reproduce the elastic and dielectric constants of the lattice. The derived potential is then validated by calculating additional bulk properties not used in the derivation procedure.

Subsequent to the derivation and validation of the potential using the pure lattice, calculated energies of intrinsic point and cluster defects are used to predict Frenkel and Schottky energies: Schottky defects are found to be the most energetically favourable form of intrinsic defect. The potential derived in this work will now be used in the atomistic simulation of cerium brannerite, $CeTi_2O_6$.

Acknowledgements

The computations described in this paper were performed using the University of Birmingham's BlueBEAR HPC service, which provides High Performance Computing to the University's research community.[1] RAB thanks The Midlands Energy Consortium for the provision of a studentship.

References

[1] World Nuclear Association, Radioactive Waste Management [online] <http://www.world-nuclear.org/information-library/nuclear-fuel-cycle/nuclear-wastes/radioactive-waste-management.aspx>.
[2] M.I. Ojovan, W.E. Lee (Eds.), Introduction to Immobilisation, In An Introduction to Nuclear Waste Immobilisation, second ed., Elsevier, Oxford, 2014.

[1] http://www.birmingham.ac.uk/bear.

[3] W.E. Lee, M.I. Ojovan, M.C. Stennett, N.C. Hyatt, Immobilisation of radioactive waste in glasses, glass composite materials and ceramics, Adv. Appl. Ceram. 105 (1) (2006) 3–12, http://dx.doi.org/10.1179/174367606X81669.
[4] F.A. Charalambous, R. Ram, M.I. Pownceby, J. Tardio, S.K. Bhargava, Chemical and microstructural characterisation studies on natural and heat treated brannerite samples, Miner. Eng. 39 (2012) 276–288, http://dx.doi.org/10.1016/j.mineng.2012.08.006.
[5] M. Colella, G.R. Lumpkin, Z. Zhang, E.C. Buck, K.L. Smith, Determination of the uranium valence state in the brannerite structure using EELS, XPS, and EDX, Phys. Chem. Miner. 32 (1) (2005) 52–64, http://dx.doi.org/10.1007/s00269-004-0444-5.
[6] J.C. Marra, A.D. Cozzi, R.A. Pierce, J.M. Pareizs, A.R. Jurgensen, D.M. Missimer, Cerium as a surrogate in the plutonium immobilized form, in: Smith, G.L. and Sundaram, S.K. and Spearing, D.R. (Ed.), Environmental Issues and Waste Management Technologies in the Ceramic and Nuclear Industries VII, vol. 132 of Ceram. Trans., Amer Ceram Soc, 2002, pp. 381–388, Symposium on Science and Technology in Addressing Environmental Issues in the Ceramic Industry/Symposium on Ceramic Science and Technology for the Nuclear Industry, INDIANAPOLIS, IN, APR 22–25, 2001.
[7] M.C. Stennett, C.L. Freeman, A.S. Gandy, N.C. Hyatt, Crystal structure and non-stoichiometry of cerium brannerite: $Ce_{0.975}Ti_2O_{5.95}$, J. Solid State Chem. 192 (2012) 172–178, http://dx.doi.org/10.1016/j.jssc.2012.03.057.
[8] S.M. Woodley, P.D. Battle, J.D. Gale, C.R.A. Catlow, The prediction of inorganic crystal structures using a genetic algorithm and energy minimisation, Phys. Chem. Chem. Phys. 1 (10) (1999) 2535–2542, http://dx.doi.org/10.1039/a901227c.
[9] G. Paglia, A.L. Rohl, C.E. Buckley, J.D. Gale, A computational investigation of the structure of kappa-alumina using interatomic potentials, J. Mater. Chem. 11 (12) (2001) 3310–3316, http://dx.doi.org/10.1039/b105664f.
[10] M.S.D. Read, R.A. Jackson, Derivation of enhanced potentials for uranium dioxide and the calculation of lattice and intrinsic defect properties, J. Nucl. Mater. 406 (3) (2010) 293–303, http://dx.doi.org/10.1016/j.jnucmat.2010.08.044.
[11] M.S.D. Read, M.S. Islam, F. King, F.E. Hancock, Defect chemistry of $La_2Ni_{1-x}M_xO_4$ (M = Mn, Fe Co, Cu): Relevance to catalytic behavior, J. Phys. Chem. B 103 (9) (1999) 1558–1562, http://dx.doi.org/10.1021/jp984059s.
[12] M.E.G. Valerio, R.A. Jackson, J.F. de Lima, Derivation of potentials for the rare-earth fluorides, and the calculation of lattice and intrinsic defect properties, J. Phys.: Condens. Matter 12 (35) (2000) 7727–7734, http://dx.doi.org/10.1088/0953-8984/12/35/308.
[13] B.G. Dick, A.W. Overhauser, Theory of the dielectric constants of alkali halide crystals, Phys. Rev. 112 (1) (1958) 90–103.
[14] N.F. Mott, M.J. Littleton, Conduction in polar crystals. 1. Electrolytic conduction in solid salts (Reprinted From, vol. 34, PG 485, 1938), J. Chem. Soc., Faraday Trans. II 85 (Part 5) (1989) 565–579.
[15] R.A. Jackson, A.D. Murray, J.H. Harding, C.R.A. Catlow, The calculation of defect parameters in UO_2, Philos. Mag. A 53 (1) (1986) 27–50.
[16] B. Vessal, M. Amini, C.R.A. Catlow, Computer-simulation of the structure of silica glass, J. Non-Cryst. Solids 159 (1–2) (1993) 184–186, http://dx.doi.org/10.1016/0022-3093(93)91295-E.
[17] M.S.D. Read, S.R. Walker, R.A. Jackson, Derivation of enhanced potentials for plutonium dioxide and the Calculation of lattice and intrinsic defect properties, J. Nucl. Mater. 448 (1–3) (2014) 20–25, http://dx.doi.org/10.1016/j.jnucmat.2014.01.020.
[18] C. Green, M.S.D. Read, Derivation of enhanced potentials for thorium dioxide, in: University of Birmingham 4th Annual BEAR PGR Conference 2013 on Research Computing, (2013) 20.
[19] J.D. Gale, GULP: capabilities and prospects, Z. Kristallogr. 220 (5–6) (2005) 552–554.
[20] E.A. Kummerle, G. Heger, The structures of C − $Ce_2O_{3+\delta}$, Ce_7O_{12}, and $Ce_{11}O_{20}$, J. Solid State Chem., 0022-4596 147 (2) (1999) 485–500, http://dx.doi.org/10.1006/jssc.1999.8403, Unique-id = ISI:000083652600007.
[21] V. Butler, C.R.A. Catlow, B.E.F. Fender, J.H. Harding, Dopant ion radius and ionic-conductivity in cerium dioxide, Solid State Ionics 8 (2) (1983) 109–113, http://dx.doi.org/10.1016/0167-2738(83)90070-X.
[22] A. Gotte, D. Spangberg, K. Hermansson, M. Baudin, Molecular dynamics study of oxygen self-diffusion in reduced CeO_2, Solid State Ionics 178 (25–26) (2007) 1421–1427, http://dx.doi.org/10.1016/j.ssi.2007.08.003.
[23] L. Minervini, M.O. Zacate, R.W. Grimes, Defect cluster formation in M_2O_3-doped CeO_2, Solid State Ionics 116 (3–4) (1999) 339–349, http://dx.doi.org/10.1016/S0167-2738(98)00359-2.
[24] S. Vyas, R.W. Grimes, D.H. Gay, A.L. Rohl, Structure, stability and morphology of stoichiometric ceria crystallites, J. Chem. Soc., Faraday Trans. 94 (3) (1998) 427–434, http://dx.doi.org/10.1039/a707052g.
[25] Z.-P. Li, T. Mori, J. Zou, J. Drennan, Optimization of ionic conductivity in solid electrolytes through dopant-dependent defect cluster analysis, Phys. Chem. Chem. Phys. 14 (23) (2012) 8369–8375, http://dx.doi.org/10.1039/c2cp40845g.
[26] P.S. Ghosh, P.S. Somayajulu, A. Arya, G.K. Dey, B.K. Dutta, Thermal expansion and thermal conductivity of $(Th, Ce)O_2$ mixed oxides: A molecular dynamics and experimental study.
[27] A. Nakajima, A. Yoshihara, M. Ishigame, Defect-Induced Raman-Spectra in Doped CeO_2, Phys. Rev. B: Condens. Matter 50 (18) (1994) 13297–13307, http://dx.doi.org/10.1103/PhysRevB.50.13297.
[28] H. Xu, R.K. Behera, Y. Wang, F. Ebrahimi, S.B. Sinnott, E.D. Wachsman, S.R. Phillpot, A critical assessment of interatomic potentials for ceria with application to its elastic properties, Solid State Ionics 181 (11–12) (2010) 551–556, http://dx.doi.org/10.1016/j.ssi.2010.02.023.
[29] S. Duclos, Y. Vohra, A. Ruoff, A. Jayaraman, G. Espinosa, High-pressure X-ray-diffraction study of CeO_2 to 70 GPa and pressure-induced phase-transformation from the fluorite structure, Phys. Rev. B: Condens. Matter 38 (11) (1988) 7755–7758, http://dx.doi.org/10.1103/PhysRevB.38.7755.
[30] L. Gerward, J.S. Olsen, L. Petit, G. Vaitheeswaran, V. Kanchana, A. Svane, Bulk modulus of CeO_2 and PrO_2 – an experimental and theoretical study, J. Alloys Compd. 400 (1–2) (2005) 56–61, http://dx.doi.org/10.1016/j.jallcom.2005.04.008.
[31] L. Gerward, J.S. Olsen, Powder diffraction analysis of cerium dioxide at high pressure, Powder Diffr. 8 (2) (1993) 127–129, http://dx.doi.org/10.1017/S0885715600017966.
[32] F. Marabelli, P. Wachter, Covalent insulator CeO_2 – optical reflectivity measurements, Phys. Rev. B: Condens. Matter 36 (2) (1987) 1238–1243, http://dx.doi.org/10.1103/PhysRevB.36.1238.
[33] N.L. Santha, M.T. Sebastian, P. Mohanan, N.M. Alford, K. Sarma, R.C. Pullar, S. Kamba, A. Pashkin, P. Samukhina, J. Petzelt, Effect of doping on the dielectric properties of cerium oxide in the microwave and far-infrared frequency range, J. Am. Ceram. Soc. 87 (7) (2004) 1233–1237.
[34] T. Gurel, R. Eryigit, Ab initio pressure-dependent vibrational and dielectric properties of CeO_2, Phys. Rev. B: Condens. Matter 74 (1) (2006), http://dx.doi.org/10.1103/PhysRevB.74.014302.
[35] F.A. Kröger, H. Vink, Relations between the concentrations of imperfections in crystalline solids, Solid State Phys. 3 (1956) 307–435.

Please cite this article in press as: R.A. Bird, M.S.D. Read, Derivation of enhanced potentials for cerium brannerite and the calculation of lattice and intrinsic defect properties, Nucl. Instr. Meth. B (2016), http://dx.doi.org/10.1016/j.nimb.2016.10.015